J Nanopart Res (2011) 13:4311–4323
DOI 10.1007/s11051-011-0378-z

RESEARCH PAPER

Multifunctional antitumor magnetite/chitosan-L-glutamic acid (core/shell) nanocomposites

Daniela P. Santos · M. Adolfina Ruiz · Visitación Gallardo · Maria Valnice B. Zanoni · José L. Arias

Received: 16 December 2010 / Accepted: 15 April 2011 / Published online: 1 May 2011

Abstract The development of anticancer drug delivery systems based on biodegradable nanoparticles has been intended to maximize the localization of chemotherapy agents within tumor interstitium, along with negligible drug distribution into healthy tissues. Interestingly, passive and active drug targeting strategies to cancer have led to improved nanomedicines with great tumor specificity and efficient chemotherapy effect. One of the most promising areas in the formulation of such nanoplatforms is the engineering of magnetically responsive nanoparticles. In this way, we have followed a chemical modification method for the synthesis of magnetite/chitosan-L-glutamic acid (core/shell) nanostructures. These magnetic nanocomposites (average size $\approx$340 nm) exhibited multifunctional properties based on its capability to load the antitumor drug doxorubicin (along with an adequate sustained release) and its potential for hyperthermia applications. Compared to drug surface adsorption, doxorubicin entrapment into the nanocomposites matrix yielded a higher drug loading and a slower drug release profile. Heating characteristics of the magnetic nanocomposites were investigated in a high-frequency alternating magnetic gradient: a stable maximum temperature of 46 °C was successfully achieved within 40 min. To our knowledge, this is the first time that such kind of stimuli-sensitive nanoformulation with very important properties (i.e., magnetic targeting capabilities, hyperthermia, high drug loading, and little burst drug release) has been formulated for combined antitumor therapy against cancer.

Keywords Biodegradable nanoparticle · Cancer · Doxorubicin · Hyperthermia · Magnetically responsive drug nanocarrier · Multifunctional nanoformulation · Nanomedicine

D. P. Santos · M. V. B. Zanoni
Institute of Chemistry, University of São Paulo State, UNESP, C.P. 355, Araraquara, SP 14801-970, Brazil

M. A. Ruiz · V. Gallardo · J. L. Arias (✉)
Department of Pharmacy and Pharmaceutical Technology, Faculty of Pharmacy, University of Granada, 18071 Granada, Spain
e-mail: jlarias@ugr.es

Introduction

Drug delivery systems are intended for enhancing the accumulation of chemotherapy agents into the targeted site of action, with a minimized biodistribution. The objective is always to protect the loaded drug from biological metabolization and elimination and to achieve the highest therapeutic effect with minimal toxicity (Arias 2008, 2011). In this way, active targeting of drugs to cancer can be made possible by the use of stimuli-sensitive drug nanocarriers and/or

through a specific recognition mechanism (ligand- or receptor-mediated targeting) (Arias 2011; Ruiz et al. 2003). The former are drug nanoformulations that can alter their physical properties under exposure to an external stimulus (e.g., magnetic gradients, light, pH, ultrasounds, enzymatic systems, etc.). This very interesting property can be exploited to trigger drug release into the targeted non-healthy tissue, but can also be utilized for a specific drug accumulation into the desired site (e.g., magnetically responsive carriers) (Arias et al. 2006; Meers 2001; Needham and Dewhirst 2001; Rapoport 2004; Torchilin 2006).

Magnetic nanoparticles are under extensive investigation to develop multifunctional nanoplatforms for the specific transport of chemotherapy agents (or genes) to malignant cells, while simultaneously inducing the death of malignant tissues by magnetic fluid hyperthermia (MFH, a property by which magnetic nanoparticles under exposure to high frequency alternating magnetic gradients, AMF, generate heat due to magnetic hysteresis loss) (Campbell 2007; Ito et al. 2005; Laurent et al. 2008; Needham et al. 2000; Tanaka et al. 2005). Such multifunctional nanoparticles (enhanced antitumor effect + hyperthermia) are expected to lead to a more selective, effective, and safety cancer treatment. Fascinatingly, MFH has been suggested to facilitate a specific triggered drug release into the tumor interstitium (Ang et al. 2007; Kalele et al. 2009; Purushotham and Ramanujan 2010), but can also enhance the accumulation of the drug delivery system into the targeted site (Jordan et al. 2001; Needham et al. 2000; Tashjian et al. 2008).

The present investigation is focussed on the preparation of magnetite/chitosan-L-glutamic acid (Fe_3O_4/CGA) (core/shell) nanocomposites loaded with the anthracycline chemotherapy agent doxorubicin [(8*S*, 10*S*)-10-(4-amino-5-hydroxy-6-methyl-tetrahydro-2*H*-pyran-2-yloxy)-6,8,11-trihydroxy-8-(2-hydroxyacetyl)-1-methoxy-7,8,9,10-tetrahydrotetracene-5, 12-dione]. The drug has been demonstrated to be effective in the treatment of neoplasms, hematopoietic malignancies, and solid tumors. Despite its very efficient anticancer activity, this chemotherapy agent generally leads to serious dose-limiting side effects especially cardiomyopathy en route to congestive heart failure and the development of drug resistance by cancer cells (Minotti et al. 2004; Sun et al. 2007). Magnetite (Fe_3O_4, mean diameter $\approx$11 nm) was chosen as a magnetic nucleus due to its very low toxicity and biocompatibility, even when coated by polymers (Iannone et al. 1991; Müller et al. 1996; Okon et al. 1994). Chitosan was used as the biocompatible and non-toxic polymeric shell onto the magnetic nanoparticles, responsible for doxorubicin vehiculization. In fact, this linear biopolyaminosaccharide has been formulated into nanoparticles both for parenteral and oral drug delivery to improve the bioavailability of degradable substances such as proteins or to enhance the uptake of hydrophilic substances across epithelial layers. The in vivo susceptibility of chitosan to lysozyme makes it biodegradable and an ideal material to provide controlled release of many drugs, such as antihypertensive agents, diuretics, anti-inflammatories, anticancer molecules, antidiabetics, antibiotics, antithrombotics, steroids, peptides, proteins, amino acids, and vaccines (Arias et al. 2010a, b; Illum 1998; Nordtveit et al. 1994; Pitt 1990; Sinha et al. 2004; Thanoo et al. 1992). Interestingly, smart strategies have been developed to tailor the in vivo solubility (and drug release) of chitosan nanoparticles, e.g., by incorporating hydrophilic molecules through chemical cross-linking (Bodnar et al. 2005; Sinha et al. 2004). This approach has been recently revisited by the use of L-glutamic acid, an amino acid with null toxicity compared to glutaraldehyde which can be easily incorporated into the chitosan chemical structure by an amide linkage between its –COOH group and the $–NH_2$ group of chitosan (Singh et al. 2009).

We have developed a reproducible procedure for the preparation of doxorubicin-loaded Fe_3O_4/CGA (core/shell) nanoparticles. The anticancer activity of this chemotherapy agent is expected to be significantly enhanced by its incorporation to this magnetic nanoformulation. The coating efficiency of the copolymer CGA around the magnetic core has been analyzed using electron microscopy, and electrical and thermodynamic surface characterizations. The amount of doxorubicin loaded to the magnetic nanocomposites either by single surface adsorption or by entrapment into the polymeric network has been investigated. The in vitro drug release profiles were also characterized according to the drug loading procedure. Spectrophotometry was validated and used successfully, as the analytical technique in the quantitative determination of both drug loading and release profiles. Drug adsorption onto the magnetic nanoparticles was also qualitatively evaluated by an electrophoretic analysis. Finally, the magnetic

properties of this multifunctional nanoformulation were characterized to analyze its magnetic responsiveness. The heating characteristics (hyperthermia effect) of the Fe_3O_4/CGA (core/shell) nanocomposites under the influence of an oscillating magnetic gradient were also investigated.

Materials and methods

Materials

All chemicals used were of analytical quality from Panreac (Spain), except for formamide, doxorubicin, low molecular weight chitosan, L-glutamic acid, and pluronic® F-68 (Sigma-Aldrich, Germany). Water used in the experiments was deionized and filtered with a Milli-Q Academic System (Millipore, France).

Methods

Preparation of magnetite/chitosan-L-glutamic acid (Fe_3O_4/CGA, core/shell) nanoparticles

A chemical co-precipitation method was followed to prepare Fe_3O_4 nuclei (Arias et al. 2008; Massart 1981). CGA nanoparticles were prepared by a chemical modification method (Singh et al. 2009). The synthesis procedure of Fe_3O_4/CGA (core/shell) nanoparticles was equal to the one followed for the preparation of the pure copolymer, except that chitosan was dissolved into an aqueous solution of acetic acid containing Fe_3O_4.

Briefly, chitosan (1%, w/v) was dissolved in 50 mL of an aqueous suspension of Fe_3O_4 nuclei (0.75%, w/v) containing 2% (v/v) acetic acid, and 1% (w/v) pluronic® F-68. 50 mL of a solution of L-glutamic acid (0.33%, w/v) was then incorporated (5 mL/min) under mechanical stirring (2000 rpm). After 6 h of continuous stirring, 25 mL of a solution of sodium sulfate (20%, w/v) was added (5 mL/min) to the polymeric solution. Mechanical stirring was continued for 1 h to obtain the aqueous suspension of magnetic CGA nanoparticles. Finally, the aqueous suspension of Fe_3O_4/CGA nanocomposites was subjected to a cleaning procedure by magnetic separation: the solids were repeatedly separated from the liquid medium using a permanent magnet (400 mT) and redispersed in pure water, until the conductivity of the supernatant was $\leq$10 μS/cm.

Doxorubicin loading to Fe_3O_4/CGA (core/shell) nanoparticles was investigated by two procedures. The entrapment method followed for drug absorption into the magnetic nanocomposites was similar to that above described for the preparation of the nanocomposites, except that the aqueous phase also included the chemotherapy agent. In this method, the influence on drug entrapment of the concentration of the antitumor molecule, the copolymer, and the stabilizing agent was investigated. To that aim, doxorubicin concentration was varied between 10^{-5} and 10^{-2} M; the chitosan (and L-glutamic acid) added to the organic phase ranged from 0.2 g (and 0.07 g) to 1 g (and 0.33 g); also, the aqueous phase (a 10^{-2} M doxorubicin solution) could contain between 0 and 2% (w/v) stabilizing agent concentration. The production performance (%) under all the formulation conditions was also determined [(amount of doxorubicin-loaded Fe_3O_4/CGA obtained (mg)/summation of materials used in the preparation of Fe_3O_4/CGA (mg)) × 100]. The second procedure (adsorption method) involved single drug surface adsorption onto preformed Fe_3O_4/CGA nanoparticles. Briefly, an aqueous suspension of magnetic nanocomposites (2%, w/v) was incubated for 24 h (at 25.0 ± 0.5 °C, and under mechanical stirring: 50 rpm) with increasing amounts of doxorubicin (up to 0.01 M).

Characterization methods

Mean particle size was determined in triplicate at 25.0 ± 0.5 °C by photon correlation spectroscopy (PCS) (Malvern Autosizer® 4700, Malvern Instruments Ltd., UK). The scattering angle was set at 60°, and the measurement was made after suitable dilution of the aqueous nanoparticle suspensions ($\approx$0.1%, w/v). The stability of the formulations was evaluated by measuring particle size after 2 weeks of storage at 4.0 ± 0.5 °C in water. To confirm these size measurements, the nanoparticles were checked through analysis by scanning electron microscopy (Zeiss DSM 950 scanning electron microscope, Germany) and by high-resolution transmission electron microscopy (HRTEM, STEM PHILIPS CM20 high resolution transmission microscope, The Netherlands). Prior to observation, dilute suspensions ($\approx$0.1%, w/v) were sonicated for 5 min, and drops were placed on copper

grids with formvar film. The grids were then dried at 25.0 ± 0.5 °C in a convection oven.

Fourier transform infrared spectrometry (Nicolet 20 SXB infrared spectrometer, USA) data with a resolution of 2 cm^{-1} were used for the chemical characterization of the three types of nanoparticles (Fe_3O_4, CGA, and core/shell nanoparticles).

The characterization of the internal structure of Fe_3O_4 and Fe_3O_4/CGA nanoparticles was performed by X-ray diffractometry, in a Philips PW1710 diffractometer (The Netherlands), using the Debye–Scherrer method with Cu K_α radiation.

The surface electrical properties of the three types of nanoparticles were analyzed by electrophoretic measurements as a function of both pH and NaCl (Malvern Zetasizer 2000 electrophoresis device, Malvern Instruments Ltd., UK). Measurements were performed at 25.0 ± 0.5 °C, after 24 h of contact at this temperature. The experimental uncertainty of the measurements was <5%. The theory of O'Brien and White was used to convert electrophoretic mobility (u_e) into zeta potential (ζ) values (O'Brien and White 1978).

A surface thermodynamic analysis of Fe_3O_4, CGA, and Fe_3O_4/CGA was also done, using the model developed by van Oss (2006), which has been shown to be very suitable in the characterization of nanoparticle surfaces (Arias et al. 2001, 2006, 2008, 2010a). The advancing contact angles of water, formamide, and diiodomethane were determined on dry nanoparticle layers (at least five layers were prepared for each liquid) (Ramé-Hart 100-00 telegoniometer, USA). Smooth surfaces were prepared by uniformly spreading a particle suspension (10% volume fraction) in carbon tetrachloride (CCl_4) on a dry and clean microscope glass slide. It was verified that spreading a volume of 2 mL of these suspensions on the slides was enough to ensure a sufficiently thick particle layer. After placing the suspensions on the slide, it was dried at 35.0 ± 0.5 °C in an oven and finally placed in a desiccator for 24 h. A macroscopically uniform layer surface was obtained, making it possible to measure contact angles on stable drops. The image of drops placed on the layers were captured with a video camera adapted to the telegoniometer, after their deposition with a Gilmont micrometer syringe (USA) which allowed a gentle deposit of droplets (≈10 μL). Contact angle measurements were done at 25.0 ± 0.1 °C inside a thermostatic chamber. At least 10 droplets were placed on the nanoparticle layers, and the average contact angle and standard deviation were calculated.

The magnetic properties of Fe_3O_4/CGA (core/shell) nanoparticles were determined at 25.0 ± 0.5 °C using a Manics DSM-8 vibrating magnetometer (France). The magnetic gradient-responsive behavior of the nanocomposites was further analyzed by optical microscope visualization of a 0.5% (w/v) aqueous suspension under exposure to a 400-mT permanent magnet (Nikon SMZ800 stereoscopic zoom microscope, Japan).

The in vitro heating behavior of the Fe_3O_4/CGA (core/shell) nanoparticles in a high-frequency alternating electromagnetic gradient was investigated in triplicate at 25.0 ± 0.5 °C. We prepare 5 mL of an aqueous suspension of the magnetic copolymer (10 mg/mL) by ultrasonication. Magnetic gradient frequency and intensity were 250 kHz and 4 kA/m, respectively. This characterization was done in triplicate at 25.0 ± 0.5 °C.

UV–Vis absorption measurements were carried out to establish doxorubicin concentration in the systems investigated at the maximum absorbance wavelength (481 nm) (8500 UV–Vis spectrophotometer, Dinko, Spain), using quartz cells (path length: 1 cm). Good linearity was observed at this wavelength, and the method was validated and verified for accuracy, precision, and linearity in all conditions tested.

Determination of doxorubicin loading to magnetite/chitosan-L-glutamic acid (Fe_3O_4/CGA, core/shell) nanoparticles

The determination of the amount of drug loaded to Fe_3O_4/CGA particles was performed in triplicate by spectrophotometric measurements of the doxorubicin remaining in the supernatant (after nanoparticle centrifugation: 40 min at 10700 rpm) which was deduced from the total amount of drug in the nanoparticle suspension (Purushotham and Ramanujan 2010). For the method to be accurate, we considered the contribution to the absorbance of sources other than variations in drug concentration (mainly, the surfactant agent), by subtracting the

absorbance of the supernatant produced in the same conditions but without the antitumor agent. Drug incorporation to nanoparticles was expressed in terms of doxorubicin loading (%) [(encapsulated drug (mg)/carrier (mg)) × 100] and doxorubicin entrapment efficiency (%) [(encapsulated drug (mg)/total drug in the nanoparticle suspension (mg)) × 100].

A qualitative follow-up of the adsorption process was done by electrophoretic mobility (u_e) determinations of Fe_3O_4/CGA (core/shell) particles in dilute suspensions (≈0.1%, w/v) with different doxorubicin concentrations. Measurements were performed at 25.0 ± 0.5 °C, after 24 h of contact at this temperature under mechanical stirring (50 rpm). The experimental uncertainty of the measurements was <5%.

In vitro release study of doxorubicin from magnetite/chitosan-L-glutamic acid (Fe_3O_4/CGA, core/shell) nanoparticles

Doxorubicin release from the magnetic nanocomposites (prepared after a single drug adsorption process, or after doxorubicin incorporation into the copolymeric shell) was investigated in triplicate at 37.0 ± 0.5 °C following the best drug loading conditions (a 10^{-2} M doxorubicin concentration in the adsorption/absorption process).

Doxorubicin release was determined in vitro following the dialysis bag method and using phosphate buffered saline (PBS, pH = 7.4 ± 0.1) as the release medium. The bags were soaked in water at 25.0 ± 0.5 °C for 12 h before use. The dialysis bag (cut-off of 2000 Da, Spectrum® Spectra/Por® 6 dialysis membrane tubing, USA) retained the magnetic nanocomposites, but allowed the free drug to diffuse into the dissolution medium. 3 mL of magnetic nanocomposite suspension (containing 3 mg/mL of doxorubicin) was placed into the dialysis bag with the two ends fixed by clamps. The bags were placed in a glass beaker containing 100 mL of PBS and stirred at 200 rpm. At prefixed time intervals (0.25, 0.5, 0.75, 1, 1.5, 2, 3, 6, 9, 24, 48, and 72 h), 5 mL of the medium was withdrawn and analyzed for the drug content using UV–Vis spectrophotometry (at 481 nm). An equal volume of PBS, maintained also at 37.0 ± 0.5 °C, was added after sample withdrawal to ensure the sink conditions. The same analytical procedure used for the quantification of doxorubicin loading was followed in this study.

Results and discussion

Particle geometry and physical chemistry

Figure 1a shows a HRTEM image of cubic Fe_3O_4 particles obtained by chemical co-precipitation (Arias et al. 2008; Massart 1981). The mean particle size (±standard deviation) and the polydispersity index were 11 ± 3 nm and 0.108, respectively. As can be observed in Fig. 1d (and 1b), magnetic Fe_3O_4/CGA (core/shell) composites are well-stabilized spherical nanoparticles with an average diameter of 340 ± 80 nm (polydispersity index: 0.191). Finally, Fig. 1c shows the spherical CGA nanoparticles (average diameter: 260 ± 35 nm and polydispersity index: 0.164). It is clear from these figures that Fe_3O_4 nuclei were very efficiently coated by a CGA copolymeric matrix: the morphology and surface of Fe_3O_4/CGA (core/shell) nanoparticles are identical to that of the pure copolymer.

The size and shape of magnetic core/shell nanoparticles, and the quality of the suspensions did not vary significantly when loaded with different amounts of doxorubicin (Table 1). Additionally, no drug precipitation or nanoparticle aggregation was observed, and no appreciable change in the size of the magnetic nanocomposites was detected by PCS after 2 weeks of storage at 4.0 ± 0.5 °C in water.

Figure 2 shows the infrared spectra of the three types of nanoparticles. The main feature of the figure is the presence of all the bands of the copolymer in the spectrum of the nanocomposites, this clearly demonstrating that the shell observed in Fig. 1b is indeed CGA coating. Interestingly, the 521 cm^{-1} band (not displayed by the pure copolymeric nanoparticles) is characteristic of Fe_3O_4 (Arias et al. 2001; Lyon 1967). Finally, Fig. 3 shows the X-ray diffraction patterns of Fe_3O_4 and Fe_3O_4/CGA nanoparticles. The comparison of both diffractograms with the ASTM pattern for Fe_3O_4 confirms the mineralogical purity of the synthesized Fe_3O_4 and its high crystallinity, even upon extensive coating by the copolymer.

Electrokinetic characterization

The electrokinetic study was first focussed on the pH effect on the zeta potential, ζ, for the three kinds of nanoparticles in the presence of 10^{-3} M NaCl (Fig. 4a). Note that Fe_3O_4 particles show a well-

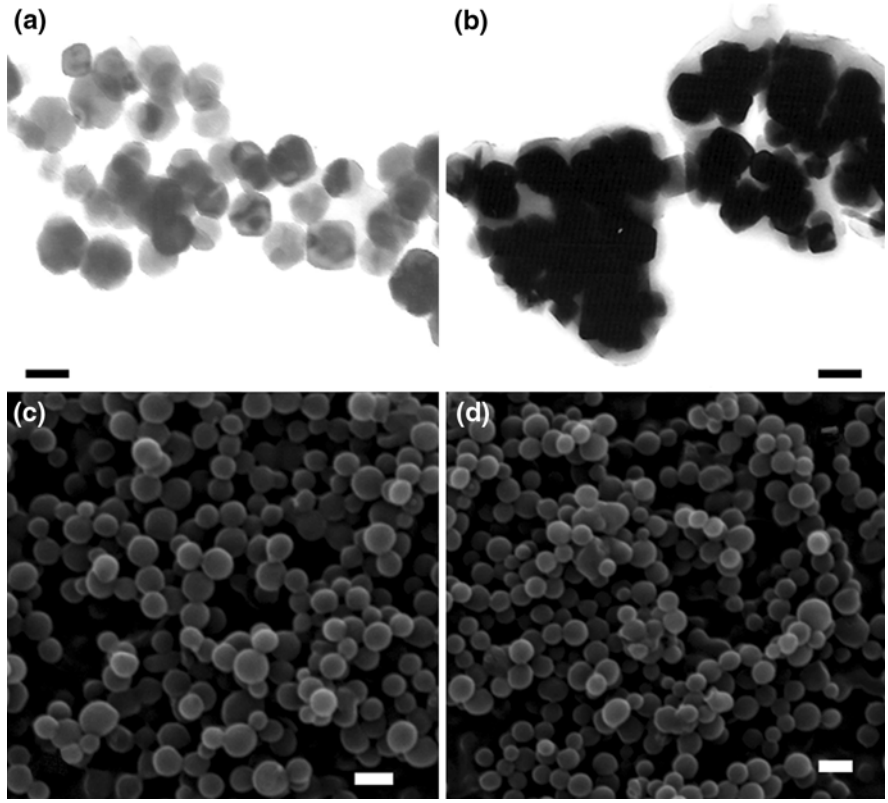

Fig. 1 High-resolution transmission electron microscopy images of magnetite (**a**) and magnetite/chitosan-L-glutamic acid (core/shell) nanoparticles (**b**). Scanning electron microscope pictures of chitosan-L-glutamic acid (**c**) and magnetite/chitosan-L-glutamic acid (core/shell) nanoparticles (**d**). *Bar lengths* 10 nm (**a** and **b**), 300 nm (**c**), and 400 nm (**d**)

Table 1 Influence of doxorubicin entrapment efficiency (%) on size of magnetite/chitosan-L-glutamic acid (core/shell) nanocomposites

Doxorubicin entrapment efficiency (%)	Size (nm)
0	340 ± 80
4.1 ± 0.9	320 ± 45
13.9 ± 1.2	345 ± 55
19.2 ± 1.3	330 ± 60
23.8 ± 3.3	360 ± 70
24.6 ± 1.9	335 ± 65

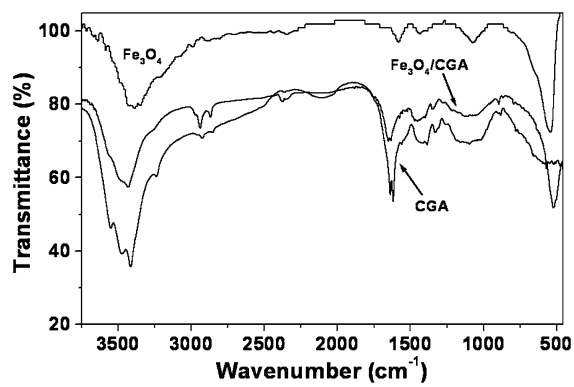

Fig. 2 Infrared spectra of magnetite (Fe_3O_4), chitosan-L-glutamic acid (CGA), and magnetite/chitosan-L-glutamic acid (Fe_3O_4/CGA) (core/shell) nanocomposites

defined isoelectric point (pH_{iep} or pH of zero potential) in the vicinity of pH 7. This result is in agreement with previous electrophoretic determinations on this material (Arias et al. 2008; Regazzoni et al. 1983). The surface charge of these iron-based nanoparticles is defined by an amphoteric thin oxide layer, whom formation cannot be avoided in oxidizing environments (Kallay et al. 1991; Plaza et al. 2002). On the opposite, CGA nanoparticles displayed a positive surface charge for the whole pH range studied. Only at pH > 9, the zeta potential could approach a zero value. CGA particles were positively charged despite sulfate ions were used as precipitant, the amide linkage between the –COOH group of L-glutamic acid and the $–NH_2$ group of chitosan (Singh et al. 2009), and even if negative groups of the dissociated pluronic® F-68 end molecules persist onto the copolymeric surface after the cleaning procedure. This indicates that only a part of the

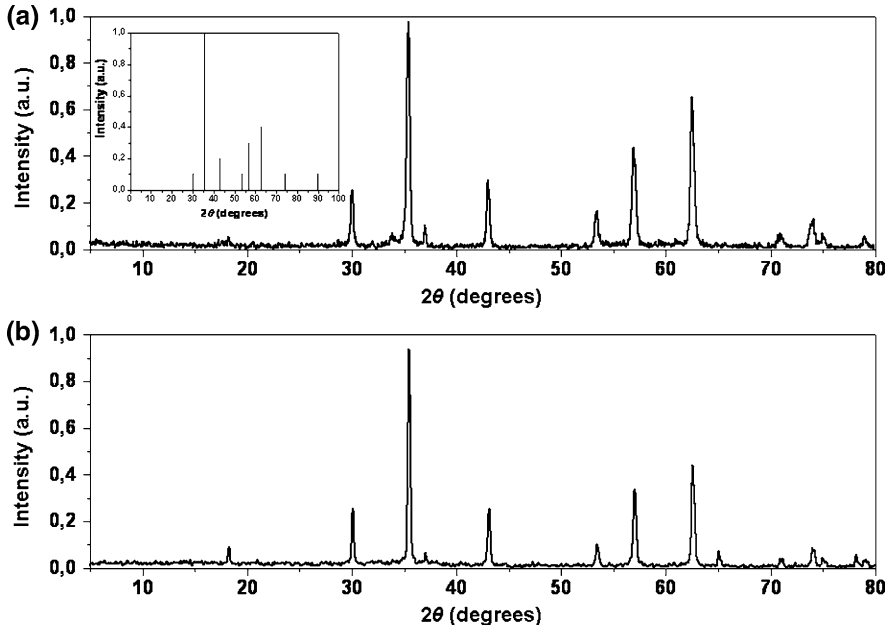

Fig. 3 X-ray diffractograms of **a** magnetite (*inset* ASTM pattern for magnetite) and **b** magnetite/chitosan-L-glutamic acid (core/shell) nanocomposites. The intensity is expressed in arbitrary units

$-NH_2$ groups were neutralized during the formation of the copolymer and, hence, the residual groups would be responsible for the positive ζ (Arias et al. 2010a).

This electrokinetic technique is a very useful tool for qualitatively checking the coating efficiency, due to the large differences between ζ of Fe_3O_4 nuclei and the CGA copolymer. In fact, Fig. 4a shows that the ζ-pH trends of Fe_3O_4/CGA (core/shell) nanoparticles are clearly dominated by the copolymeric shell. This must be the consequence of an efficient copolymeric coating of Fe_3O_4, leading to nanocomposites which are qualitatively similar to CGA from an electrokinetic point of view.

This conclusion was confirmed by measuring ζ as a function of NaCl concentration at a constant pH 5 (Fig. 4b). Note that the effect of NaCl concentration on each of the nanoparticles is different. As it is observed, the Fe_3O_4/CGA nanocomposites yield ζ values almost indistinguishable to those of the copolymer. Of a greater interest is the fact that the absolute value of ζ changes differently with the ionic strength: a decrease in $|\zeta|$ of pure CGA and Fe_3O_4/CGA nanoparticles was observed when NaCl concentration was increased. This is the consequence of the classical double-layer compression mechanism, in virtue of which the electric potential decreases faster with distance, the larger the ionic strength is (Arias et al. 2008). On the opposite, pure Fe_3O_4 nanoparticles displayed a different trend: $|\zeta|$ slightly went through a maximum ($\approx 10^{-3}$ M NaCl), so that only at high enough NaCl concentration was the double-layer compression slightly observed. This is supposed to be a manifestation of stagnant-layer conductivity (Arias et al. 2008; Lyklema 2002).

Surface thermodynamics and mechanism of formation of the copolymeric layer

The analysis of the surface-free energy components (γ_S) of the three types of nanoparticles was used to check the nature of the copolymeric coating. The contact angle data of the three probe liquids on dry nanoparticle layers already suggest significant differences among the three materials (Fig. 5a). However, it is the evaluation of the γ_S components which provides a better characterization of the nanoparticle surface thermodynamics (Fig. 5b). As can be seen, whatever the component considered, its values for the nanocomposites are similar to those for the bare copolymer. For instance, γ_S^- shows large values in Fe_3O_4 (a monopolar, electron-donor material) than that found for either the copolymer or the core/shell composites. Thus, the thermodynamic analysis agrees with the electrokinetic one in suggesting that sufficient coverage of Fe_3O_4 nuclei has been achieved, since the γ_S components of nanocomposites coincide almost exactly with those corresponding to CGA.

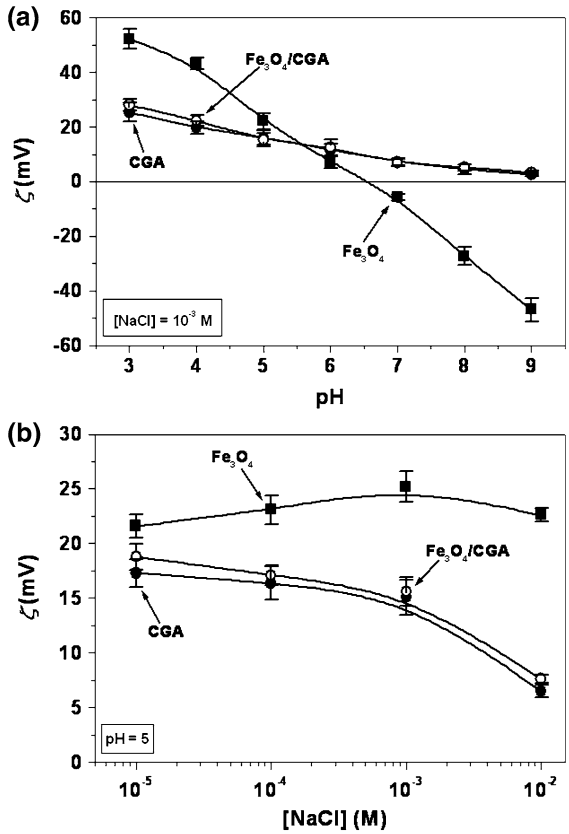

Fig. 4 Zeta potential of magnetite (Fe_3O_4, *filled square*), chitosan-L-glutamic acid (CGA, *filled circle*), and magnetite/chitosan-L-glutamic acid (Fe_3O_4/CGA, *open circle*) (core/shell) nanoparticles as a function of pH in the presence of 10^{-3} M NaCl (**a**) and as a function of the NaCl concentration at pH = 5 (**b**). The lines are guides to the eye

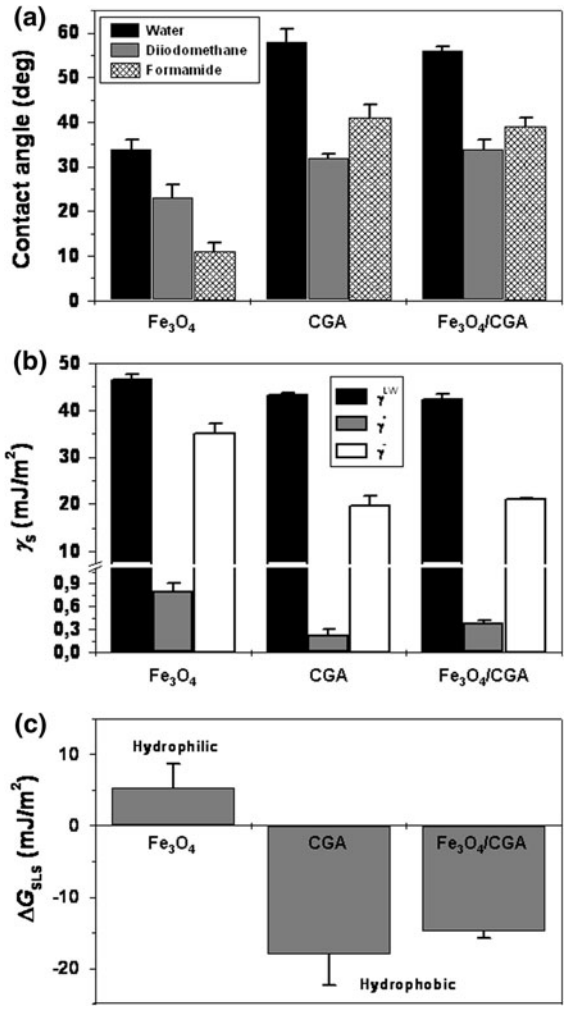

Fig. 5 **a** Contact angle θ (°) of the liquids indicated on magnetite (Fe_3O_4), chitosan-L-glutamic acid (CGA), and magnetite/chitosan-L-glutamic acid (Fe_3O_4/CGA) (core/shell) nanocomposites. **b** Surface-free energy components (mJ/m^2) of Fe_3O_4, CGA, and Fe_3O_4/CGA nanoparticles. γ_S^{LW} is the Lifshitz–van der Waals component; γ_S^+ (γ_S^-) is the electron-acceptor (electron-donor) component. **c** ΔG_{SLS} (solid–liquid interfacial energy of interaction) values (mJ/m^2) and hydrophobicity/hydrophilicity of the three types of nanoparticles

These surface-free energy changes manifest themselves in the hydrophobicity/hydrophilicity properties of the materials. The evaluation of the free energy of interaction, not considering the electrostatic component, between the solid phases immersed in the liquid (ΔG_{SLS}^{TOT}) can be used to check whether a material is hydrophobic or hydrophilic (Arias et al. 2009; van Oss 2006). This quantity is negative for hydrophobic materials, where interfacial interactions will favor attraction of the nanoparticles to each other. Oppositely, hydrophilicity will correspondingly be associated to positive values of ΔG_{SLS}^{TOT}. As observed in Fig. 5c, the hydrophilic nature of Fe_3O_4 is modified and the core becomes hydrophobic (just like the copolymer) when covered by CGA.

Finally, the surface thermodynamic data may also help to investigate the mechanism by which the CGA layer deposited onto the Fe_3O_4 surface. From γ_S data, the free energy of interaction between Fe_3O_4 (M) and CGA (C) in the aqueous medium (A), ΔG_{MAC}, can be calculated using the Dupré equation (Arias et al. 2008; van Oss 2006). The result of the calculation was -4.7 ± 0.4 mJ/m^2. This means that the van der Waals and acid–base interactions between Fe_3O_4 and CGA were neatly attractive. In other words, it was thermodynamically favorable for the copolymer to

remain adsorbed onto Fe_3O_4 nanoparticles rather than as isolated entities in water.

Magnetic properties

The magnetic responsiveness of the Fe_3O_4/CGA (core/shell) nanocomposites was determined by the hysteresis cycle (Fig. 6a). The soft magnetic character of the nanocomposite is apparent in this figure, as the increasing and decreasing field branches of the hysteresis cycle are hardly distinguishable with the sensitivity of the instrument used. From the linear portions (low field) of the curve, we could estimate the initial susceptibility, $\chi_i = 0.69 \pm 0.07$ and the saturation magnetization: 70.3 ± 1.8 kA/m for the Fe_3O_4/CGA nanoparticles.

The response of Fe_3O_4/CGA nanocomposites to an external magnetic gradient of 400 mT was evaluated by optical microscopy inspection of the corresponding aqueous suspension. Interestingly, the initially homogeneous distribution of particles in the magnetofluid (Fig. 6b) was strongly modified, and formation of chainlike aggregates parallel to the gradient lines occurred (Fig. 6c). This is due to the fact that the magnetic interaction represents a significant contribution over the DLVO colloidal interactions between Fe_3O_4/CGA nanoparticles (electrostatic van der Waals and hydration or acid–base), in spite of the presence of the copolymeric shell.

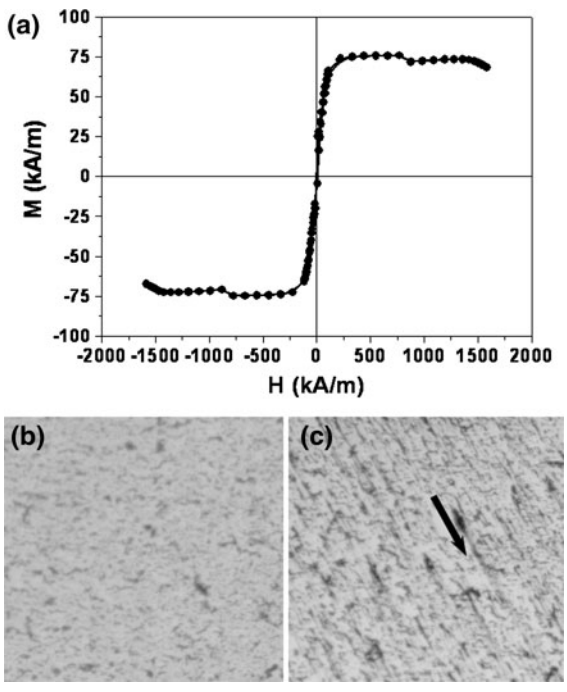

Fig. 6 **a** Hysteresis cycle of the magnetite/chitosan-L-glutamic acid (core/shell) nanocomposites. Optical microscope photographs (magnification ×63) of a core/shell nanoparticle aqueous suspension without (**b**) and under the influence (**c**) of an external magnetic gradient, $B = 400$ mT, in the direction of the arrow

In vitro heating behavior in an alternating magnetic gradient

Figure 7 shows the in vitro heating behavior of a Fe_3O_4/CGA magnetofluid (10 mg/mL) in a high-frequency oscillating magnetic gradient. Under exposure to the alternating electromagnetic gradient, the oscillation of the magnetic moment of the Fe_3O_4/CGA nanocomposites transforms them into heaters that can produce heat up to ≈46 °C. It has been shown that tumor cells are irreversibly damaged at this temperature, and locally heating a tumor tissue for ≈30 min is enough to destroy it (Huber 2005).

As can be observed in the figure, the temperature rises from room temperature and reaches the minimum hyperthermia temperature (≈41 °C) in 20 min. Under the experimental conditions, the maximum temperature reaches 46 °C after 40 min and then stabilized until the end of the experiment. This proves a good control of the temperature and heat flux, a basic requirement for hyperthermia application. Particularly, if we keep in mind that when the temperature rises out of control (>48 °C), it is hypothesized

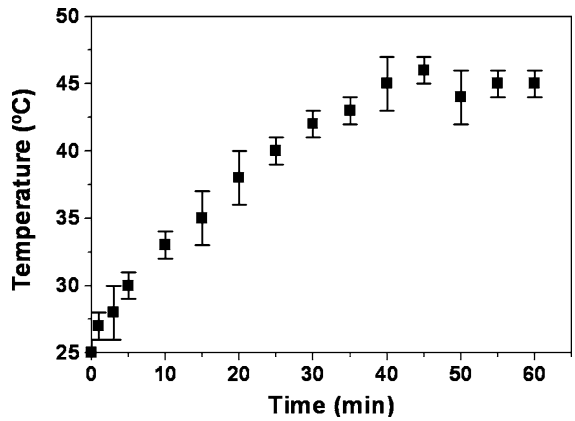

Fig. 7 Heating curve of a magnetite/chitosan-L-glutamic acid (core/shell) magnetofluid (10 mg/mL) exposed to a high-frequency alternating electromagnetic gradient. Magnetic gradient frequency and intensity: 250 kHz and 4 kA/m, respectively

that healthy tissues surrounding the tumor site will be burn and damaged (Lao and Ramanujan 2004).

Doxorubicin surface adsorption

Following the adsorption procedure, almost negligible drug incorporation onto the surface of the Fe_3O_4/CGA nanoparticles was obtained. Although doxorubicin adsorption efficiency was positively influenced by the drug concentration in the incubation medium, the maximum entrapment efficiency (%) and drug loading (%) of doxorubicin were $\approx$4.2% and $\approx$0.4% for the range of concentrations investigated (up to 0.01 M), respectively. These results could be explained if we consider that the interaction between the drug [under a non-ionized form: pK_a (8.6) > pH of the adsorption medium ($\approx$5.0)] (Gaihre et al. 2009) and the positively charged CGA surface (see Fig. 4a) will not be electrostatically favoured. Electrophoretic mobility (u_e) measurements qualitatively confirmed the conclusions based on adsorption determinations. u_e displayed a non-significant trend to rise toward progressively more positive values as the doxorubicin concentration was increased.

Doxorubicin absorption

The formulation conditions tried to minimize the escape of the drug from the CGA shell of the nanocomposites: the Fe_3O_4/CGA nanoparticles precipitated immediately after the beginning of the chemical modification method (Singh et al. 2009). Thus, it is expected to lead to an enhanced mechanical trapping of doxorubicin within the copolymeric matrix. Compared to drug adsorption, a high drug loading is supposed to take place because the stabilizing agent (pluronic® F-68) is supposed to induce the opening of the polymeric chains, thus creating a space within the CGA matrix where doxorubicin can be incorporated (Arias et al. 2010a, b; Llovet et al. 1995; Soppimath et al. 2001).

Figure 8 shows the amount of antitumor molecule absorbed into the Fe_3O_4/CGA nanocomposites as a function of the drug concentration. Compared to the surface adsorption procedure, both the entrapment efficiency (%) and the drug loading (%) were significantly increased whatever the initial doxorubicin concentration fixed. For instance, when the initial drug concentration in the adsorption/absorption medium was 10^{-2} M, these parameters rise from $\approx$4.2% and $\approx$0.4% (after doxorubicin adsorption onto the nanocomposite surface) to $\approx$24.6% and $\approx$12.1% (when the chemotherapy agent was absorbed into the CGA matrix), respectively. In addition, a positive effect of doxorubicin concentration on the absorption efficiency into the Fe_3O_4/CGA nanoparticles was observed.

Regarding the effect of the surfactant concentration on the doxorubicin loading, the addition of pluronic® F-68 to the aqueous phase yielded homogeneous distributions of magnetic (core/shell) nanoparticles with reduced size and great uniformity, and better drug entrapment efficiencies (Table 2) (Arias et al. 2007, 2010a, b). Interestingly, the production performance of doxorubicin-loaded Fe_3O_4/CGA nanoparticles was always >93% in all the formulations tested, and only falls to <11% when no stabilizing

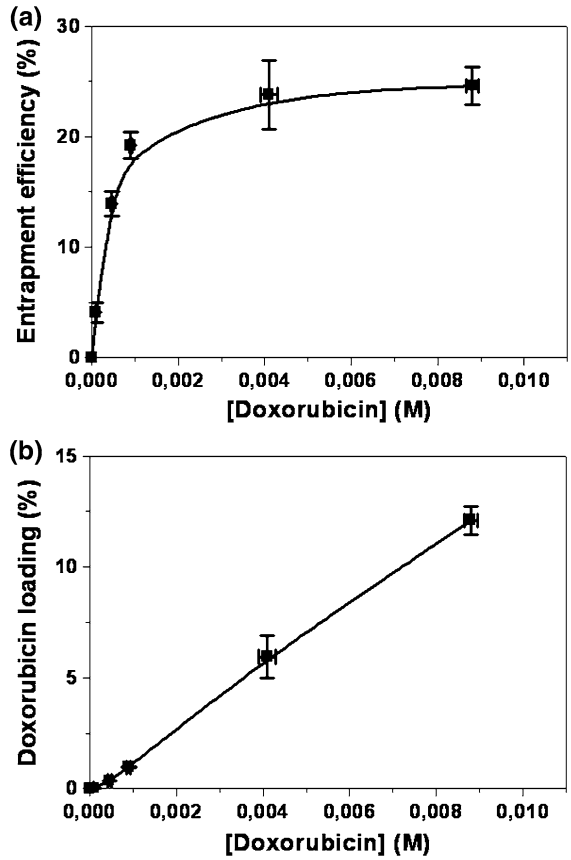

Fig. 8 Doxorubicin entrapment efficiency (%) (**a**) and doxorubicin loading (%) (**b**) values into magnetite/chitosan-L-glutamic acid (core/shell) nanocomposites, as a function of the drug concentration. The lines are guides to the eye

Table 2 Influence of the copolymer and surfactant concentrations on size, and doxorubicin entrapment efficiency (%) into magnetite/chitosan-L-glutamic acid (core/shell) nanocomposites

Copolymer (%, w/v)	Pluronic® F-68 (%, w/v)	Size (nm) and polydispersity index	Drug entrapment efficiency (%)
0.5	1	330 ± 55, 0.156	24.9 ± 3.2
1	1	335 ± 65, 0.167	24.6 ± 1.9
2	1	360 ± 60, 0.184	25.4 ± 2.3
1	0	815 ± 280, 0.542	7.3 ± 1.8
1	0.5	350 ± 50, 0.139	25.1 ± 2.4
1	2	345 ± 70, 0.166	24.4 ± 2.6

In the formulation of the drug-loaded magnetic nanocomposites, doxorubicin concentration was fixed to be 0.01 M

agent was added to the aqueous phase. Finally, neither the concentration of pluronic® F-68 nor the amount of copolymer solubilized into the precipitation medium influenced significantly the doxorubicin entrapment efficiency (Table 2) (Arias et al. 2010a, b; Llovet et al. 1995; Soppimath et al. 2001).

In vitro release of doxorubicin

The release of doxorubicin adsorbed onto Fe_3O_4/CGA nanoparticles was almost complete after ≈2 h, due to a single and very rapid desorption process from the copolymeric surface (Fig. 9). Regarding the release of the chemotherapy molecule absorbed into the Fe_3O_4/CGA nanocomposites, it is apparent from the figure that the release profile was a biphasic process, with an initial fast (burst) drug release (up to ≈30% in ≈1 h), the remaining doxorubicin being released in a sustained manner during ≈71 h (≈3 days). The burst drug release is presumably due to the leakage of the surface-associated and/or poorly entrapped drug, which easily diffuses in the initial incubation time. Then, the rate of doxorubicin release fell as the dominant release mechanism is probably changed to drug diffusion through the copolymeric matrix (Papadimitriou et al. 2008). Such a biphasic profile suggests that the major fraction of doxorubicin was entrapped into the copolymeric network rather than adsorbed onto the nanocomposite surface.

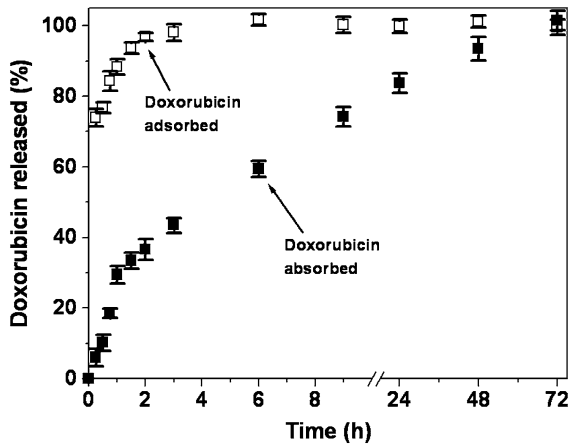

Fig. 9 Release of doxorubicin adsorbed (*open square*) or absorbed (*filled square*) from magnetite/chitosan-L-glutamic acid (core/shell) nanocomposites as a function of the incubation time in PBS (pH = 7.4 ± 0.1) at 37.0 ± 0.5 °C

Conclusions

In this study, we have developed a magnetically responsive nanocomposite in which magnetite nanocores are very efficiently coated by a chitosan-L-glutamic acid copolymer. These core/shell nanoparticles may constitute a potential candidate for combined cancer treatment: they are tailored to deliver appropriate amounts of the antitumor drug doxorubicin specifically into the cancer site, in combination with a selective hyperthermia effect into the tumor region.

Acknowledgments Financial support from project PE2008-FQM-3993 (Junta de Andalucía) is acknowledged. D.P. Santos also gratefully acknowledges the financial support of FAPESP (research fellowship: process no. 2007/07914-7).

References

Ang KL, Venkatraman S, Ramanujan RV (2007) Magnetic PNIPA hydrogels for hyperthermia applications in cancer therapy. Mater Sci Eng C 27:347–351. doi:10.1016/j.msec.2006.05.027

Arias JL (2008) Novel strategies to improve the anticancer action of 5-fluorouracil by using drug delivery systems. Molecules 13:2340–2369. doi:10.3390/molecules13102340

Arias JL (2011) Drug targeting strategies in cancer treatment: an overview. Mini Rev Med Chem 11:1–17. doi:10.2174/138955711793564024

Arias JL, Gallardo V, Gómez-Lopera SA, Plaza RC, Delgado AV (2001) Synthesis and characterization of poly(ethyl-2-cyanoacrylate) nanoparticles with a magnetic core. J Control Release 77:309–321. doi:10.1016/S0168-3659(01)00519-3

Arias JL, Gallardo V, Linares-Molinero F, Delgado AV (2006) Preparation and characterization of carbonyl iron/poly (butylcyanoacrylate) core/shell nanoparticles. J Colloid Interface Sci 299:599–607. doi:10.1016/j.jcis.2006.03.005

Arias JL, Gallardo V, Ruiz MA, Delgado AV (2007) Ftorafur loading and controlled release from poly(ethyl-2-cyanoacrylate) and poly(butylcyanoacrylate) nanospheres. Int J Pharm 337:282–290. doi:10.1016/j.ijpharm.2006.12.023

Arias JL, Reddy LH, Couvreur P (2008) Magnetoresponsive squalenoyl gemcitabine composite nanoparticles for cancer active targeting. Langmuir 24:7512–7519. doi:10.1021/la800547s

Arias JL, Reddy LH, Couvreur P (2009) Polymeric nanoparticulate system augmented the anticancer therapeutic efficacy of gemcitabine. J Drug Target 17:586–598. doi:10.1080/10611860903105739

Arias JL, Martínez-Soler GI, López-Viota M, Ruiz MA (2010a) Formulation of chitosan nanoparticles loaded with metronidazole for the treatment of infectious diseases. Lett Drug Des Discov 7:70–78. doi:10.2174/157018010790225831

Arias JL, López-Viota M, Gallardo V, Ruiz MA (2010b) Chitosan nanoparticles as a new delivery system for the chemotherapy agent tegafur. Drug Dev Ind Pharm 36:744–750. doi:10.3109/03639040903517914

Bodnar M, Hartmann JF, Borbely J (2005) Preparation and characterization of chitosan-based nanoparticles. Biomacromolecules 6:2521–2527. doi:10.1021/bm0502258

Campbell RB (2007) Battling tumors with magnetic nanotherapeutics and hyperthermia: turning up the heat. Nanomedicine 2:649–652. doi:10.2217/17435889.2.5.649

Gaihre B, Khil MS, Lee DR, Kim HY (2009) Gelatin-coated magnetic iron oxide nanoparticles as carrier system: drug loading and in vitro drug release study. Int J Pharm 365:180–189. doi:10.1016/j.ijpharm.2008.08.020

Huber DL (2005) Synthesis, properties, and applications of iron nanoparticles. Small 1:482–501. doi:10.1002/smll.200500006

Iannone A, Magin RL, Walczack T, Federico M, Swartz HM, Tomasi A, Vannini V (1991) Blood clearance of dextran magnetite particles determined by a noninvasive in vivo ESR method. Magn Reson Med 22:435–442. doi:10.1002/mrm.1910220251

Illum L (1998) Chitosan and its use as a pharmaceutical excipient. Pharm Res 15:1326–1331. doi:10.1023/A:1011929016601

Ito A, Shinkai M, Honda H, Kobayashi T (2005) Medical application of functionalized magnetic nanoparticles. J Biosci Bioeng 100:1–11. doi:10.1263/jbb.100.1

Jordan A, Scholz R, Maier-Hauff K, Johannsen M, Wust P, Nadobny J, Schirra H, Schmidt H, Deger S, Loening S, Lanksch W, Felix R (2001) Presentation of a new magnetic field therapy system for the treatment of human solid tumors with magnetic fluid hyperthermia. J Magn Magn Mater 225:118–126. doi:10.1016/S0304-8853(00)01239-7

Kalele S, Narain R, Krishnan KM (2009) Probing temperature-sensitive behavior of pNIPAAm-coated iron oxide nanoparticles using frequency-dependent magnetic measurements. J Magn Magn Mater 321:1377–1380. doi:10.1016/j.jmmm.2009.02.134

Kallay N, Torbić Ž, Golić M, Matijević E (1991) Determination of the isoelectric points of several metals by an adhesion method. J Phys Chem 95:7028–7032. doi:10.1021/j100171a056

Lao LL, Ramanujan RV (2004) Magnetic and hydrogel composite materials for hyperthermia applications. J Mater Sci Mater Med 15:1061–1064. doi:10.1023/B:JMSM.0000046386.78633.e5

Laurent S, Forge D, Port M, Roch A, Robic C, Elst LV, Muller RN (2008) Magnetic iron oxide nanoparticles: synthesis, stabilization, vectorization, physicochemical characterizations, and biological applications. Chem Rev 108:2064–2110. doi:10.1021/cr068445e

Llovet MI, Egea MA, Valero J, Alsina MA, García ML, Chauvet A (1995) Methotrexate-loaded nanoparticles: analysis of drug content and study of the matrix structure. Drug Dev Ind Pharm 21:1761–1771. doi:10.3109/03639049509069263

Lyklema J (2002) The role of surface conduction in the development of electrokinetics. In: Delgado AV (ed) Interfacial electrokinetics and electrophoresis. Marcel Dekker, New York, pp 87–98

Lyon RJP (1967) Infrared absorption spectroscopy. In: Zussman J (ed) Physical methods in determinative mineralogy. Academic Press, London/New York, pp 371–399

Massart R (1981) Preparation of aqueous magnetic liquids in alkaline and acidic media. IEEE Trans Magn 17:1247–1248. doi:10.1109/TMAG.1981.1061188

Meers P (2001) Enzyme-activated targeting of liposomes. Adv Drug Deliv Rev 53:265–272. doi:10.1016/S0169-409X(01)00205-8

Minotti G, Menna P, Salvatorelli E, Cairo G, Gianni L (2004) Anthracyclines: molecular advances and pharmacologic developments in antitumor activity and cardiotoxicity. Pharmacol Rev 56:185–229. doi:10.1124/pr.56.2.6

Müller RH, Maaßen S, Weyhers H, Specht F, Lucks JS (1996) Cytotoxicity of magnetite-loaded polylactide, polylactide/glycolide particles and solid lipid nanoparticles. Int J Pharm 138:85–94. doi:10.1016/0378-5173(96)04539-5

Needham D, Dewhirst MW (2001) The development and testing of a new temperature-sensitive drug delivery system for the treatment of solid tumors. Adv Drug Deliv Rev 53:285–305. doi:10.1016/S0169-409X(01)00233-2

Needham D, Anyarambhatla G, Kong G, Dewhirst MW (2000) A new temperature-sensitive liposome for use with mild hyperthermia: characterization and testing in a human tumor xenograft model. Cancer Res 60:1197–1201

Nordtveit RJ, Vårum KM, Smidsrød O (1994) Degradation of fully water-soluble, partially *N*-acetylated chitosans with lysozyme. Carbohydr Polym 23:253–260. doi:10.1016/0144-8617(94)90187-2

O'Brien RW, White LR (1978) Electrophoretic mobility of a spherical colloidal particle. J Chem Soc Faraday Trans 2:1607–1626. doi:10.1039/F29787401607

Okon E, Pouliquen D, Okon P, Kovaleva ZV, Stepanova TP, Lavit SG, Kudryavtsev BN, Jallet P (1994)

Biodegradation of magnetite dextran nanoparticles in the rat: a histologic and biophysical study. Lab Invest 71:895–903

Papadimitriou S, Bikiaris D, Avgoustakis K, Karavas E, Georgarakis M (2008) Chitosan nanoparticles loaded with dorzolamide and pramipexole. Carbohydr Polym 73:44–54. doi:10.1016/j.carbpol.2007.11.007

Pitt CG (1990) The controlled parenteral delivery of polypeptides and proteins. Int J Pharm 59:173–196. doi:10.1016/0378-5173(90)90108-G

Plaza RC, Arias JL, Espín M, Jiménez ML, Delgado AV (2002) Aging effects in the electrokinetics of colloidal iron oxides. J Colloid Interface Sci 245:86–90. doi:10.1006/jcis.2001.7964

Purushotham S, Ramanujan RV (2010) Thermoresponsive magnetic composite nanomaterials for multimodal cancer therapy. Acta Biomater 6:502–510. doi:10.1016/j.actbio.2009.07.004

Rapoport N (2004) Combined cancer therapy by micellar-encapsulated drug and ultrasound. Int J Pharm 277:155–162. doi:10.1016/j.ijpharm.2003.09.048

Regazzoni AE, Blesa MA, Maroto AJG (1983) Interfacial properties of zirconium dioxide and magnetite in water. J Colloid Interface Sci 91(2):560–570. doi:10.1016/0021-9797(83)90370-3

Ruiz MA, Gallardo V, Arias JL, Delgado A (2003) Effect of latex and plasticizer concentration on glucocorticoid release from ointments. Pharm Ind 65:454–457

Singh J, Dutta PK, Dutta J, Hunt AJ, Macquarrie DJ, Clark JH (2009) Preparation and properties of highly soluble chitosan-L-glutamic acid aerogel derivative. Carbohydr Polym 76:188–195. doi:10.1016/j.carbpol.2008.10.011

Sinha VR, Singla AK, Wadhawan S, Kaushik R, Kumria R, Bansal K, Dhawan S (2004) Chitosan microspheres as a potential carrier for drugs. Int J Pharm 274:1–33. doi:10.1016/j.ijpharm.2003.12.026

Soppimath KS, Aminabhavi TM, Kulkarni AR, Rudzinski WE (2001) Biodegradable polymeric nanoparticles as drug delivery devices. J Control Release 70:1–20. doi:10.1016/S0168-3659(00)00339-4

Sun JB, Duan JH, Dai SL, Ren J, Zhang YD, Tian JS, Li Y (2007) In vitro and in vivo antitumor effects of doxorubicin loaded with bacterial magnetosomes (DBMs) on H22 cells: the magnetic bio-nanoparticles as drug carriers. Cancer Lett 258:109–117. doi:10.1016/j.canlet.2007.08.018

Tanaka K, Ito A, Kobayashi T, Kawamura T, Shimada S, Matsumoto K, Saida T, Honda H (2005) Heat immunotherapy using magnetic nanoparticles and dendritic cells for T-lymphoma. J Biosci Bioeng 100:112–115. doi:10.1263/jbb.100.112

Tashjian JA, Dewhirst MW, Needham D, Viglianti BL (2008) Rationale for and measurement of liposomal drug delivery with hyperthermia using non-invasive imaging techniques. Int J Hyperth 24:79–90. doi:10.1080/02656730701840147

Thanoo BC, Sunny MC, Jayakrishnan A (1992) Cross-linked chitosan microspheres: preparation and evaluation as a matrix for the controlled release of pharmaceuticals. J Pharm Pharmacol 44:283–286

Torchilin VP (2006) Multifunctional nanocarriers. Adv Drug Deliv Rev 58:1532–1555. doi:10.1016/j.addr.2006.09.009

van Oss CJ (2006) Interfacial forces in aqueous media, 2nd edn. CRC Press, Boca Raton, FL